CHINESE OPTICS LETTERS

Vol. 22, No. 3 | March 2024

Simple real-time high-sensitivity heterodyne coherent optical transceiver at intraplane satellite communication

Yuanzhe Qu (曲元哲), Qianwu Zhang (张倩武)*, Yanyi Wang (王演祎), Yanhao Chen (陈彦昊), Lewei Gong (龚乐为), Ziyue Liu (刘紫玥), Junjie Zhang (张俊杰), Yingchun Li (李迎春), Jian Chen (陈 健), and Yingxiong Song (宋英雄)**

Key Laboratory of Specialty Optics and Optical Access Networks, Shanghai Institute for Advanced Communication and Data Science, Shanghai University, Shanghai 200444, China

*Corresponding author: zhangqianwu@shu.edu.cn

**Corresponding author: herosf@shu.edu.cn

Received September 27, 2023 | Accepted November 4, 2023 | Posted Online March 21, 2024

In this paper, we demonstrate a high-sensitivity and real-time heterodyne coherent optical transceiver for intraplane satellite communication, without digital-to-analog converter (DAC) devices and an optical phase lock loop (OPLL). Based on the scheme, a real-time sensitivity of −49 dBm is achieved at 5 Gbps QPSK. Because DAC is not needed at the transmitter, as well as OPLL at the receiver, this reduces the system cost. Furthermore, the least required Rx ADC bit-width is also discussed. Through theoretical analysis and experimental results, our cost-effective transceiver satisfies the scenario and could be a promising component for future application.

Keywords: real-time coherent transceiver; heterodyning; intraplane satellite optical communication.

DOI: 10.3788/COL202422.030601

1. Introduction

The satellite optical communication network has become a promising core network structure and has attracted many commercial companies, including SpaceX, OneWeb, and Telesat. It aims to deploy thousands of low Earth orbit (LEO) satellites to provide high-speed and low-latency global broadband services[1–3]. Up till now, many satellite optical communication field tests have been successfully demonstrated, such as LEO-GND[4,5], LEO-LEO[6], LEO-GEO[7], and GEO-GND[8]. Based on these, several satellite optical network programs have been raised[9,10].

Meanwhile, with the introduction of coherent optical techniques, it is possible to realize large-capacity satellite communication[11–14]. In Ref. [15], a 160 Gbps single-channel polarization-division multiplexing—quadrature phase-shift keying (PDM-QPSK) intersatellite transmission at 40,000 km has been simulated. And in Ref. [16], a 100 to 600 Gbps 16-QAM WDM system over 5000 km transmission was also verified through software simulation. As for practical tests, in Ref. [17], a 13.16 Tbps 54-channel DWDM free-space optical data transmission over 10.45 km was demonstrated. While in a recent report, a single-carrier 0.94 Tbps with polarization-multiplexed high-order complex modulation formats over 53.42 km transmission has been realized by employing a full adaptive optics system[18]. However, besides the communication performance, the costs for the design of satellite transceivers should also be considered. Traditional coherent optical transceivers could be costly in an LEO scenario. Yet the low-cost IM/DD system, another transceiver structure widely used in the LEO-GND scenario, cannot provide enough sensitivity in some long-distance LEO-LEO communication situations. Therefore, in order to establish a network consisting of thousands of satellites, it is essential to further simplify the coherent transceiver design.

In this Letter, we propose an advanced and simple scheme of coherent optical transceiver for satellite communication without digital-to-analog converters (DACs) and an optical phase lock loop (OPLL). In our scheme, the DACs at the transmitter are replaced by a pair of DC blocks. On the other hand, a low-noise erbium-doped optical fiber amplifier (EDFA) is used as the pre-amplifier and a heterodyne receiver is used to detect the signal. The target link budget is analyzed, and the numerical receiver noise model is discussed. Through real-time experimental results, the bit error rate (BER) of the 5 Gbps QPSK signal can reach below the hard-decision forward-error-correction (HD-FEC) threshold of 3.8×10^{-3} at the received optical power (ROP) of −49 dBm. Based on our proposed scheme, the DAC is not needed, and the heterodyne receiver is applied in place of the common homodyne or intradyne receiver. This not only reduces the system cost but also shows a comparable sensitivity performance. And the least ADC bit-width requirement is further discussed through offline processing to simplify the transceiver. We believe that our proposed scheme is a promising design for intersatellite optical communication.

2. System Setup Design

2.1. Link budget analysis

To discuss the link budget of intersatellite optical communication, the average ROP P_r can be estimated as[19,20]

$$P_r = P_t \cdot G_t \cdot \eta_t \cdot L_R \cdot G_r \cdot \eta_r \cdot L_{\mathrm{pr}}, \tag{1}$$

where P_t denotes the transmitted optical power; G_t denotes the Tx optical antenna gain; η_t denotes the Tx optical system efficiency; L_R denotes the free-space link loss; G_r denotes the Rx optical antenna gain; η_r denotes the Rx optical system efficiency; and L_{pr} denotes the pointing loss.

The Tx optical antenna gain G_t can be calculated by

$$G_t = 8\left(\frac{\pi\omega}{\lambda}\right)^2, \tag{2}$$

where $\omega = \lambda/(\pi \cdot \tan\theta_{\mathrm{div}})$ is the beam radius and θ_{div} is the beam divergence angle; λ is the optical wavelength.

The free-space link loss L_R is given by

$$L_R = \left(\frac{\lambda}{4\pi R}\right)^2, \tag{3}$$

where R is the link distance.

The Rx optical antenna gain G_r is shown by

$$G_r = \left(\frac{\pi D}{\lambda}\right)^2, \tag{4}$$

where D is the Rx optical antenna diameter.

The pointing loss L_{pr} is estimated by

$$L_{\mathrm{pr}} \approx e^{-8\left(\frac{\theta_{\mathrm{off}}}{\theta_{\mathrm{div}}}\right)^2}, \tag{5}$$

where θ_{off} is the off-axis error angle.

As shown in Table 1, the intraplane link distance can be roughly summarized as between 1000 and 5000 km. Taking into consideration other parameters in Table 2, the theory ROP shown in Fig. 1 ranges from −30 to −44 dBm. Therefore, the basic sensitivity requirement should be at least below −44 dBm.

Table 1. Link Distances for Intraplane Satellite Links[21].

Project	Intraplane Link Distance
Telesat	5200 km
SpaceX	700 km
OneWeb	1200 km

Table 2. Link Parameters.

Parameter	Value
Wavelength	1550 nm
Tx & Rx aperture diameter	8 cm[1]
Pointing accuracy	2.0 μrad[1]
Tx power	1 W[1]
Tx & Rx optical system efficiency	0.5

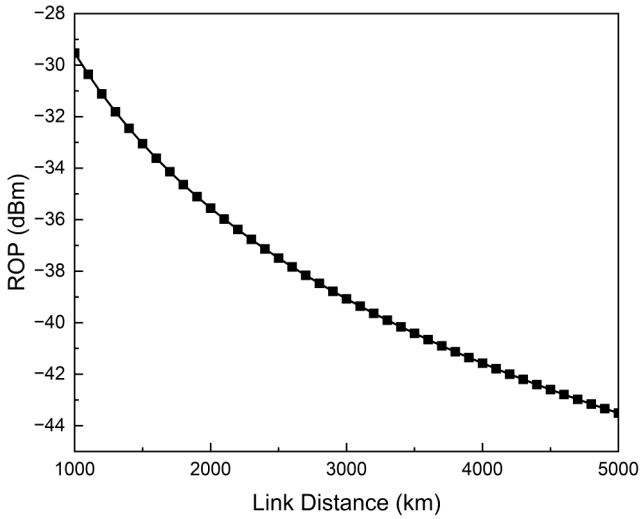

Fig. 1. Requirement for ROP at different link distances.

2.2. Transceiver scheme

The block diagram of the proposed scheme is represented in Fig. 2(a). The transmitter is composed of an external cavity laser (ECL), an IQ modulator, a modulator bias controller (MBC), an EDFA booster, two DC blocks, and two driving amplifiers. The transmitted bits are directly output from the service processor without pulse formation. The DAC is replaced by a pair of DC blocks. Two driving amplifiers are used to amplify the electrical signal, which is ready to be modulated through the IQ modulator. The MBC here is used to control the bias of the IQ modulator. The modulated optical signal is then boosted by the EDFA and sent to the Tx optical antenna. The receiver side consists of an ECL, an EDFA (which acts as a pre-amplifier), an optical bandpass filter (BPF), and a coherent receiver. The received signal is amplified by a low-noise EDFA. Extra-band noise induced from the EDFA is filtered by a normal WDM optical filter. After being detected by a commercial integrated coherent receiver (ICR), the electrical signal is sampled by an ADC and processed by the digital signal processing (DSP) module. The optical part prototype (without EDFAs) is shown in Fig. 2(b).

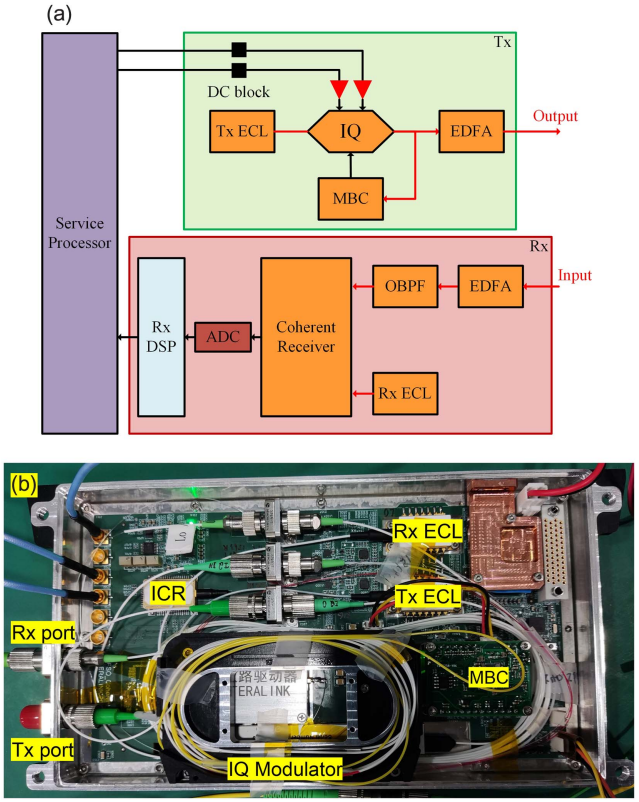

Fig. 2. Schematic of the transceiver. (a) Block diagram; (b) optical part prototype.

In the traditional coherent optical transceiver used in satellite communication systems, the DAC is indispensable. However, the DAC is expensive and has a large power consumption. In addition, different from normal homodyne receivers, we choose the heterodyne structure to decrease the application of the OPLL. The OPLL is a complicated backfeed design that needs precise control, which increases the cost of the transceiver. Thanks to our proposed scheme, the DAC and OPLL are no longer required.

For frequency offset, since the Doppler shift in the intraplane scenario is relatively small, actual frequency offset is simply estimated by the frequency recovery module in Rx DSP. If the offset exceeds our DSP compensation range of ±300 MHz, the local oscillator (LO) wavelength will be adjusted by varying the current of Rx ECL (LO) temperature controller according to a premade control instruction. And as long as the offset is within ±1 GHz, it can be adjusted automatically.

2.3. Receiver noise analysis

The electric field of the received signal can be given by

$$E_s(t) = \sqrt{\frac{P_s}{2}} \exp\, j[2\pi f_s t + \theta_s(t) + \theta_{\mathrm{ns}}(t)], \tag{6}$$

where $P_s = P_r$ denotes the average ROP from the optical antenna; f_s denotes the carrier frequency; $\theta_s(t)$ denotes the modulation phase; and $\theta_{\mathrm{ns}}(t)$ denotes the signal noise phase.

The LO is expressed as

$$E_{\mathrm{LO}}(t) = \sqrt{\frac{P_{\mathrm{LO}}}{2}} \exp\{j[2\pi f_{\mathrm{LO}} t + \theta_{\mathrm{nLO}}(t)]\}, \tag{7}$$

where P_{LO} is the LO average power; and $\theta_{\mathrm{nLO}}(t)$ is the LO noise phase.

As shown in Fig. 2(a), in our designed heterodyne receiver, the expression of the output photocurrent is written as

$$i(t) = R\sqrt{GP_sP_{\mathrm{LO}}}\, \cos[(\omega_s - \omega_{\mathrm{LO}})t + \theta_s(t) + \theta_n(t)], \tag{8}$$

where $\theta_n(t) = \theta_{\mathrm{ns}}(t) - \theta_{\mathrm{nLO}}(t)$; G represents the pre-amplifier gain; and R is the PD responsivity.

The average power of the photocurrent is given as

$$|i_c|^2 = 0.5R^2GP_sP_{\mathrm{LO}}. \tag{9}$$

On the other hand, the noise of each pair of BPDs mainly comes from three aspects[22].

(i) The shot noise, which is

$$\overline{i_{\mathrm{shot}}^2} = 2eR\frac{P_{\mathrm{LO}}}{2}B, \tag{10}$$

where e denotes the electron charge, and B denotes the noise bandwidth corresponding to the symbol rate.

(ii) The ASE-LO beat noise, which is

$$\overline{i_{\mathrm{beat}}^2} = 4eR\frac{\eta(G-1)n_{\mathrm{sp}}}{2}\frac{P_{\mathrm{LO}}}{2}B, \tag{11}$$

where $n_{\mathrm{sp}} > 1$ denotes the spontaneous radiation factor, and $P_{\mathrm{LO}}/2$ denotes the LO power into the BPD. It is worth mentioning that the power has been halved during the phase diversity process.

(iii) The circuit noise, which is

$$\overline{i_{\mathrm{circuit}}^2} = \frac{4kT}{R_{\mathrm{in}}}B, \tag{12}$$

where kT is the thermal energy, and $R_{\mathrm{in}} = 50\,\Omega$ is the input resistance.

The total noise of the photocurrent is the sum of the three kinds of noise above,

$$\overline{i_n^2} = \overline{i_{\mathrm{shot}}^2} + \overline{i_{\mathrm{beat}}^2} + \overline{i_{\mathrm{circuit}}^2}. \tag{13}$$

Then we get the signal-to-noise ratio (SNR) expression,

$$\gamma_s = \frac{|i_c|^2}{\overline{i_n^2}}. \tag{14}$$

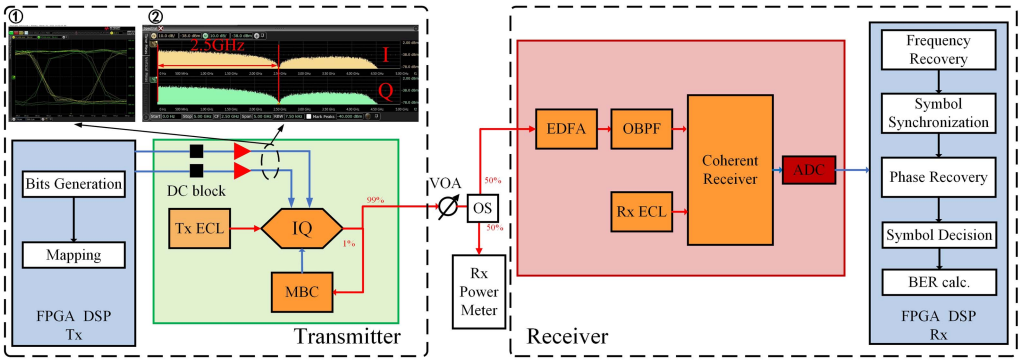

Fig. 3. Experimental setup.

3. Experimental Setup and Results

The experimental setup of our proposed scheme is depicted in Fig. 3. The Tx and Rx laser diodes are both ECL with 10 kHz linewidth and 10 dBm optical power. PRBS15 bit sequence is generated by a field-programmable gate array (FPGA) without pulse shaping. After the DC blocks, the eye diagram and real-time spectrum are captured by a real-time digital storage oscilloscope (DSO) and are shown in the illustrations in Fig. 3. After modulation, the optical signal is then sent to a VOA to simulate the transmission power loss, taking into consideration that the intersatellite link is an ideal channel. A 50:50 optical splitter (OS) is used to observe the ROP.

At the receiver side, as demonstrated in Section 2.2, after being pre-amplified by a low-noise EDFA, the signal is converted to electrical domain by a commercial coherent receiver with 25 GHz bandwidth. The electrical signal is sampled and quantized by a 10 GSa/s ADC with 8-bit bit-width. It is worth noting that the system is all-polarization-maintained, and there is no extra polarization-induced signal damage. Important experimental details are shown in Table 3.

Table 3. Experimental Parameters.

Parameter	Value
Wavelength	1540.56 nm (uplink)
	1563.05 nm (downlink)
Data rate	5 Gbps QPSK
Tx & Rx ECL power	10 dBm
Tx & Rx ECL linewidth	10 kHz
Code pattern	PRBS15
EDFA NF	4 dB
ADC sampling rate	10 GSa/s
ADC bit-width	8-bit

The digital samples captured from the ADC are processed in an FPGA, where a set of DSP subsystems is applied to compensate for the channel noise and retrieve the transmitted signal information. The first stages of DSP are aimed at frequency recovery, including downconversion and frequency offset compensation. Next, the symbol synchronization is performed with the inserted pilots, which are the fixed 16 QPSK symbols sequence. After downsampling from the synchronization, carrier-phase recovery is realized. In Fig. 4, the error vector magnitude (EVM) is evaluated between the recovered constellation and the standard QPSK constellation. As the ROP decreases from −46 dBm to −50 dBm, the constellation points become more dispersed, and the EVM increases by 9.88%. Further, we calculated the E_b/N_0, and the theoretical value here is deduced according to Section 2.3. The E_b/N_0 is improved with the increase of the ROP. It can be seen that there is a deviation of about 2 dB between the theoretical value and our platform test result. This could be due to the additional loss caused by sampling quantization error and imperfect DSP recovery.

To reflect the communication performance directly, we calculate the real-time bidirectional communication BER performance according to Figs. 5(a) and 5(b). Figure 6 shows the

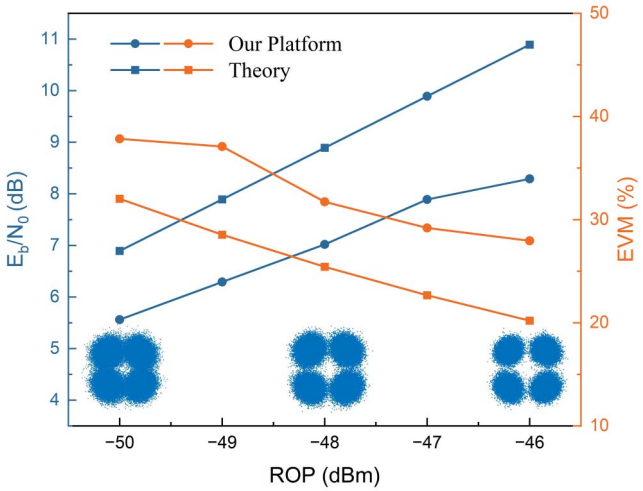

Fig. 4. E_b/N_0 and EVM versus ROP.

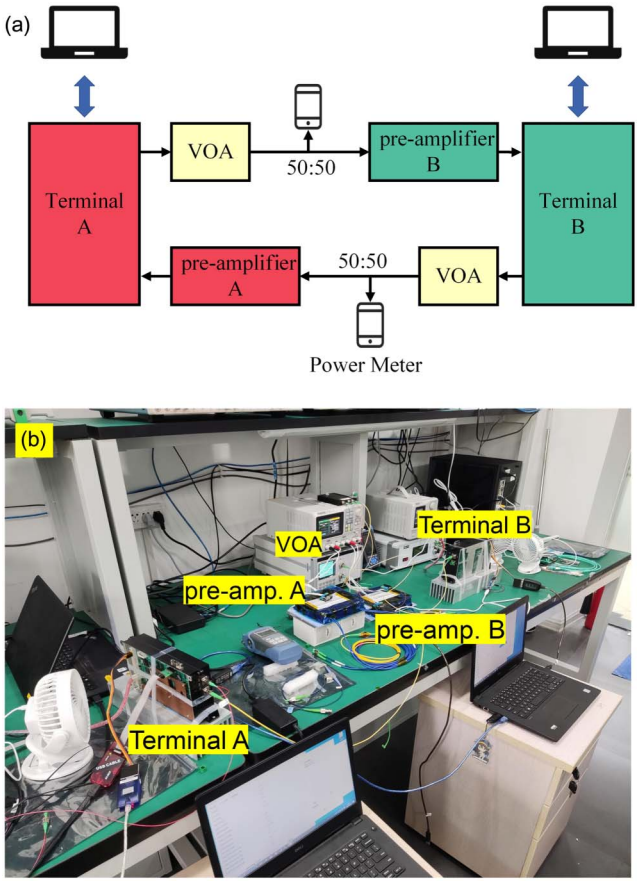

Fig. 5. Real-time bidirectional experimental setup. (a) Block diagram; (b) indoor ob2b experimental environment.

sensitivity curve to achieve a target BER of 3.8×10^{-3} (HD-FEC limit). From the results, the sensitivity of our designed transceiver reaches −49 dBm with 5 Gbps QPSK. It perfectly satisfies the real intersatellite optical communication scenario discussed in Section 2.1, leaving an extra 5 dB redundancy. And if higher performance FEC code like low density parity check (LDPC) code is applied, the sensitivity of this transceiver could be decreased to −50 dBm and below. In addition, the average power consumption of our prototypes is stable at 43–44 W during the bidirectional communication test. Moreover, taking the reality that the ROP may be below −49 dBm into account, we provide two additional data rates, 2.5 Gbps BPSK and 1.25 Gbps BPSK, with the minimum sensitivity of about −55 dBm for backup.

Furthermore, based on the sampling before, we discuss the minimum required ADC bit-width of the transceiver. Through offline DSP, the results of the BER versus the ROP under different sampling bit-widths are shown in Fig. 7. When the bit-width decreases, the sensitivity performance becomes significantly worse. And the limit ADC bit-width is 4-bit with sensitivity of −44 dBm, which satisfies the basic requirement of the real link discussed in Section 2.1. To some extent, this can save the power and DSP resource consumption and reduce the component cost.

In Table 4, several real-time free-space optical (FSO) coherent communication transceivers are listed. To evaluate the sensitivity performance fairly, the results are discussed with respect to photons per bit (PPB). It can be found that the homodyne system has the advantage of extra-low sensitivity at a relatively low data rate. However, the BPSK homodyne transceiver requires the OPLL, which increases the complexity and cost. In order to avoid applying the OPLL, an autodyne transceiver can be a choice in the DPSK system. Yet when the modulation order increases, the intradyne transceiver, also known as a digital homodyne transceiver, becomes the mainstream design but needs a pair of DACs to output the Tx signal for the pulse-forming process. Compared with other published work, our real-time heterodyne transceiver without DAC and OPLL exhibits a comparable sensitivity with other systems and further reduces the cost. In the future, higher data rates will be required for

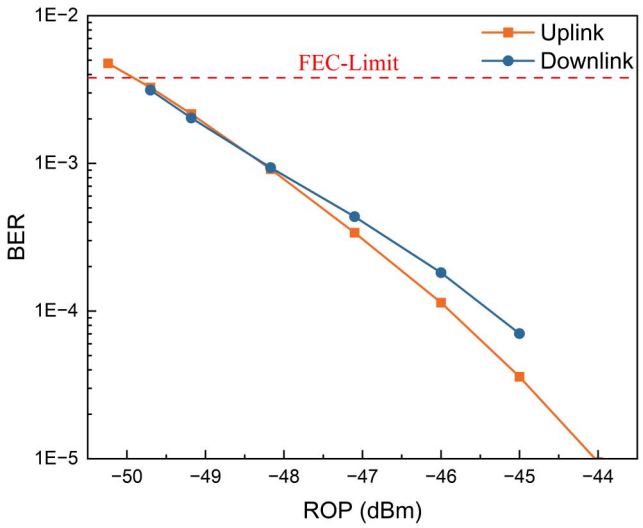

Fig. 6. Real-time 5 Gbps QPSK bidirectional BER performance.

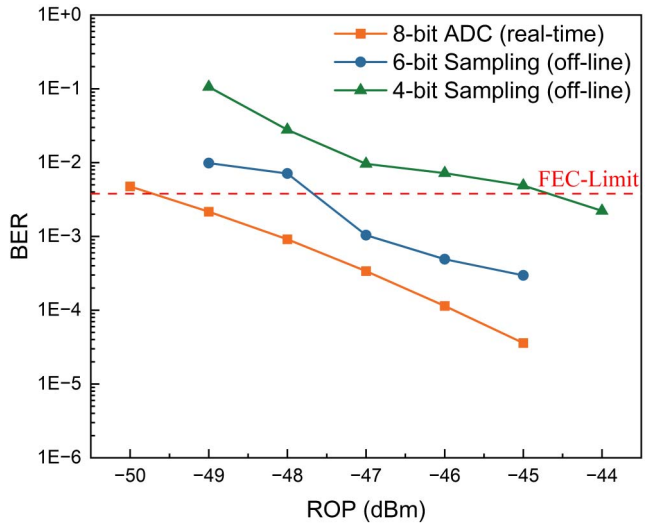

Fig. 7. BER performance with different ADC bit-widths.

Table 4. Performance of Different Published Real-Time FSO Coherent Transceivers.

Structure	Modulation	Data Rate	Sensitivity	PPB	DAC	OPLL	Reference
Homodyne	BPSK	1 Gbps	−59.2 dBm	9.89 dB	No	Yes	[23]
Homodyne	BPSK	5.625 Gbps	≈−43 dBm	18.39 dB	No	Yes	[24]
Autodyne	DPSK	2.88 Gbps	≈−52 dBm	12.30 dB	No	No	[25]
Intradyne	DP-QPSK	10 Gbps	−37.2 dBm	21.76 dB	Yes	No	[26]
Heterodyne	QPSK	5 Gbps	−49 dBm	12.9 dB	No	No	This work

commercial satellite optical communication. And based on our scheme, high-order modulation like QAM-16 or QAM-64 with the same baud rate as the prototype could be a promising way to increase the transmission rate without too much hardware change.

Reference [24] does not mention sensitivity directly; here, we deduce the result from the transmission distance of about 3700–4700 km according to Section 2.1. The real sensitivity performance could be better.

4. Conclusion

In this paper, a novel scheme of high-sensitivity heterodyne optical transceiver without DAC and OPLL for intraplane satellite communication is proposed and experimentally demonstrated. The analytical and experimental results prove the feasibility of our proposed scheme. Based on our scheme, 5 Gbps QPSK real-time bidirectional communication is realized with a sensitivity of −49 dBm at the HD-FEC limit. And we prove that the Rx ADC bit-width can be further reduced to 4-bit. Moreover, our heterodyne transceiver without DAC and OPLL reduces the system cost significantly. We believe the proposed transceiver is a promising component for intersatellite optical communication.

Acknowledgements

This work was supported in part by the National Key Research and Development Program of China (No. 2021YFB2900800), the Science and Technology Commission of Shanghai Municipality (Nos. 22511100902, 22511100502, 20511102400, and 20ZR1420900), and the 111 Project (No. D20031).

References

1. I. D. Portillo, B. G. Cameron, and E. F. Crawley, "A technical comparison of three low earth orbit satellite constellation systems to provide global broadband," Acta Astronaut. **159**, 123 (2019).
2. O. Kodheli, E. Lagunas, N. Maturo, *et al.*, "Satellite communications in the new space era: a survey and future challenges," IEEE Commun. Surv. Tutor. **23**, 70 (2020).
3. H. Kaushal and G. Kaddoum, "Optical communication in space: challenges and mitigation techniques," IEEE Commun. Surv. Tutor. **19**, 57 (2016).
4. M. Reyes, Z. Sodnik, P. Lopez, *et al.*, "Preliminary results of the in-orbit test of ARTEMIS with the optical ground station," Proc. SPIE **4635**, 38 (2002).
5. T. S. Rose, S. W. Janson, S. LaLumondiere, *et al.*, "LEO to ground optical communications from a small satellite platform," Proc. SPIE **9354**, 93540I (2015).
6. T. Tolker-Nielsen and G. Oppenhaeuser, "In orbit test result of an operational optical intersatellite link between ARTEMIS and SPOT4, SILEX," Proc. SPIE **4635**, 1 (2002).
7. H. Zech, F. Heine, D. Tröndle, *et al.*, "LCT for EDRS: LEO to GEO optical communication at 1,8 Gbps between Alphasat and Sentinel 1a," Proc. SPIE **9647**, 96470J (2015).
8. V. Cazaubiel, G. Planche, V. Chorvalli, *et al.*, "LOLA: a 40.000 km optical link between an aircraft and a geostationary satellite," Proc. SPIE **10567**, 1056726 (2017).
9. D. Calzolaio, F. Curreli, J. Duncan, *et al.*, "EDRS-C: the second node of the European Data Relay System is in orbit," Acta Astronaut. **177**, 537 (2020).
10. M. Toyoshima, "Recent trends in space laser communications for small satellites and constellations," J. Lightwave Technol. **39**, 693 (2021).
11. H. Wang, X. Yi, J. Zhang, *et al.*, "Extended study on equalization-enhanced phase noise for high-order modulation formats," J. Lightwave Technol. **40**, 7808 (2022).
12. F. Li, D. Zou, W. Ni, *et al.*, "Transmission and reception of 17× 480 Gbit/s PDM-16QAM with Tx/Rx I/Q imbalance compensation and simplified MLSE for metro-regional 400G optical communications," in *Optical Fiber Communication Conference (OFC)* (2023), paper Th1E-2.
13. X. Wang, Z. Chen, M. Yin, *et al.*, "Laser sharing uplink polarization division multiplexing FBMC passive optical network," J. Lightwave Technol. **41**, 2323 (2022).
14. W. Ren, J. Sun, P. Hou, *et al.*, "Direct phase control method for binary phase-shift keying space coherent laser communication," Chin. Opt. Lett. **20**, 060601 (2022).
15. P. Sivakumar, M. Singh, J. Malhotra, *et al.*, "Performance analysis of 160 Gbit/s single-channel PDM-QPSK based inter-satellite optical wireless communication (IsOWC) system," Wirel. Netw. **26**, 3579 (2020).
16. M. R. Djellouli, S. A. Chouakri, and A. Ghaz, "OWC inter satellite link throughput improvement based on WDM architecture," in *2nd International Conference on Advanced Electrical Engineering (ICAEE)* (2022), p. 1.
17. A. Dochhan, J. Poliak, J. Surof, *et al.*, "13.16 Tbit/s free-space optical transmission over 10.45 km for geostationary satellite feeder-links," in *Photonic Networks 20th ITG Symposium* (2019), p. 1.
18. Y. Horst, B. I. Bitachon, L. Kulmer, *et al.*, "Tbit/s line-rate satellite feeder links enabled by coherent modulation and full-adaptive optics," Light Sci. Appl. **12**, 153 (2023).
19. J. Liang, A. U. Chaudhry, E. Erdogan, *et al.*, "Link budget analysis for free-space optical satellite networks," in *IEEE 23rd International Symposium on a World of Wireless, Mobile and Multimedia Networks (WoWMoM)* (2022), p. 471.
20. H. Kotake, Y. Abe, M. Sekiguchi, *et al.*, "Link budget design of adaptive optical satellite network for integrated non-terrestrial network," in *IEEE*

International Conference on Space Optical Systems and Applications (ICSOS) (2022), p. 240.
21. C. Carrizo, M. Knapek, J. Horwath, *et al.*, "Optical inter-satellite link terminals for next generation satellite constellations," Proc. SPIE **11272**, 1127203 (2020).
22. K. Kikuchi and S. Tsukamoto, "Evaluation of sensitivity of the digital coherent receiver," J. Lightwave Technol. **26**, 1817 (2008).
23. C. Yue, J. Li, J. Sun, *et al.*, "Homodyne coherent optical receiver for intersatellite communication," Appl. Opt. **57**, 7915 (2018).
24. K. Böhmer, M. Gregory, F. Heine, *et al.*, "Laser communication terminals for the European data relay system," Proc. SPIE **8246**, 82460D (2012).
25. M. A. Krainak, E. Luzhanskiy, S. X. Li, *et al.*, "A dual format communication modem development for the Laser Communications Relay Demonstration (LCRD) program," Proc. SPIE **8610**, 86100K (2013).
26. R. Matsumoto, K. Matsuda, M. Hosokawa, *et al.*, "10-Gb/s laser communication demonstration based on digital coherent technique," in *IEEE International Conference on Space Optical Systems and Applications (ICSOS)* (2017), p. 172.